3.1. THE MISTRAL AT THE EXIT OF THE RHONE VALLEY

Philippe Drobinski[1,*], Sophie Bastin[1], Vincent Guénard[2], Jean-Luc Caccia[2], Alain M. Dabas[3], Patricia Delville[4], Alain Protat[1], Oliver Reitebuch[5], Christian Werner[5]

(1) IPSL, Paris, France; (2) LSEET, La Garde, France; (3) CNRM/Météo-France, Toulouse, France; (4) DT/INSU, Meudon, France; (5) DLR, Wessling, Germany

1. INTRODUCTION

During the 28 June 2001 Mistral case documented in the framework of the ESCOMPTE (Expérience sur Site pour COntraindre les Modèles de Pollution atmosphériques et de Transport d'Emissions) field experiment in southern France (Cros et al. 2004) (Fig. 1), the french-german airborne Doppler lidar WIND was flown and could map in three dimension the Mistral wind at the exit of the Rhône valley (jets and wakes) and the associated planetary boundary layer (PBL) structure (depth), as never done before. These measurements were complemented with thermodynamical measurements by radiosondings, surface stations and mesoscale numerical simulations using the Penn State –National Center for Atmospheric Research MM5 model. They provided an unprecedented insight in mesoscale dynamics of the Mistral.

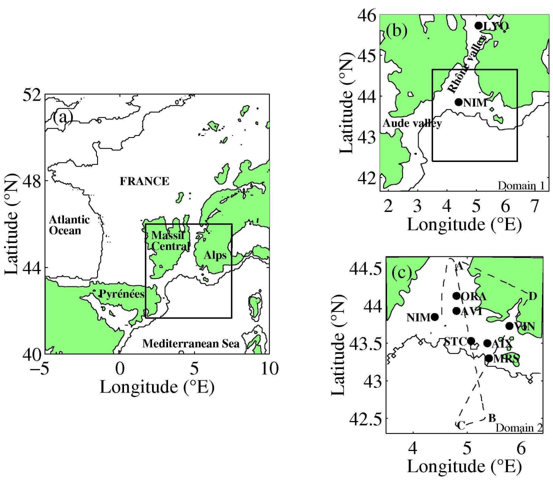

Fig. 1: Panel~a: Map of France with the topography shaded in grey when higher than 500 m above sea level. The rectangle displays the large domain (domain 1) of the MM5 simulations. Panel b: Domain 1 of the MM5 simulation with its nested smaller domain (domain 2) in the rectangle. The acronyms NIM and LYO stand for Nîmes and Lyon, respectively. Panel c: Domain 2 of the MM5 simulation. The dashed line corresponds to the flight track of the DLR Falcon 20 carrying the Doppler lidar WIND. The acronyms AIX, MRS, STC and VIN correspond to Aix en Provence, Marseille, Saint Chamas and Vinon, respectively.

* Corresponding author address: Dr. Philippe Drobinski, IPSL/SA, Université Pierre et Marie Curie, Paris, France.
Tel : 33+1.69.33.31.99
e-mail : philippe.drobinski@aero.jussieu.fr

2. LIDAR AND NUMERICAL SIMULATIONS

2.1 *Airborne 10.6 µm Doppler lidar WIND*

The french-german airborne Doppler lidar WIND was operated on the 28 June 2001 Mistral case between 1016 and 1041 UTC. The lidar is operated at 10.6 µm in the infrared spectral region and was on board of the Falcon 20 of the DLR (Werner et al. 2001). It flew along the tracks shown in Fig. 1c at an altitude of 6.5 km with an aircraft ground speed of around 170 m s^{-1}. The Doppler lidar WIND provides wind profiles, obtained by conically scanning the line-of-sight (LOS) around the vertical axis with a fixed angle of 30° from na dir. The profile of the wind vector are calculated from the LOS wind speeds using a velocity-azimuthal display (VAD) technique. A full scan revolution of the line-of-sight takes 20 s, leading to a horizontal resolution of about 3.4 km between vertical profiles of the wind vector. The vertical resolution of the wind profiles is 250 m and the accuracy of the horizontal wind velocity is better than 1 m s^{-1}. A 3D variational analysis (Scialom et al. 1990) was also applied to the high-resolution horizontal wind profiles derived from WIND to provide a three dimensional wind field on a regular horizontal grid bounded by the flight tracks.

2.2 *MM5 simulations*

The numerical simulations presented in this study have been conducted with the Penn State - National Center for Atmospheric Research MM5 model, version 3.6 (Grell 1995). Two interactively nested model domains are used, the horizontal mesh size being 9 km and 3 km, respectively (see Fig. 1). In the vertical, 43 unevenly spaced sigma-levels are used. The lowermost level is about 12 m above ground. The vertical distance between the model levels is about 50 m close to the ground and increases up to 1000 m near the upper boundary which is located at 100 hPa. A complete set of physics parametrization is used. The initial and boundary conditions are taken from the operational ECMWF (European Centre for Medium Range Weather Forecast) analyses. The initialization date is 27 June 2001 at 1200 UTC and the simulation ends on 29 June 2001 at 0600 UTC.

3. SYNOPTIC ENVIRONMENT

The 28 June 2001 Mistral event is featured by a zonal flow over the Atlantic Ocean resulting from an anticyclone over Spain and low-pressure system over northern Atlantic. After the passage of a cold front, a surface low is generated (1008 hPa) in the wake of the Alps ridge marking the onset of the Mistral wind due to the Genoa cyclogenesis process. On 28 June 2001 in the morning, a high-pressure zone (1020 hPa) coming from Spain is moving eastward and strengthens northwesterly winds over the Mediterranean. The Mediterranean cyclone (1010 hPa) also moves eastward and is centered over Corsica at 1200 UTC. During the afternoon, the high-pressure zone moves northeastwardly and its center is located over France, deflecting the Atlantic air masses toward the North Sea. On 29 June 2001, the Genoa cyclone weakens and moves southeastward over southern Italy (1016 hPa), while a high pressure increases over the Balearic Isles (1022 hPa). This results in the cessation of the Mistral wind.

4. JET STRUCTURE AND WAKE GENERATION AT THE RHONE VALLEY EXIT

4.1 *Flow description*

The simulated and observed wind fields on 28 June 2001 at 1000 UTC and at 500 m AGL are displayed in Fig. 2 and show the complexity of the Mistral flow. The Mistral wind originates from the north end of the Rhône valley with a cyclonic curvature and extends beyond the south boundary of the inner domain. The western boundary of the Mistral is defined by a wake trailing downstream the Massif Central. Within this large wake, regions of alternating higher- and lower-wind speed form three secondary potential vorticity banners. The three narrow wakes part of the larger wake form in the lee of the Mont Mézenc (peak culminating at 1754 m corresponding to the northernmost wake), the Mont Lozère (peak culminating at 1702 m corresponding to the middle wake) and the Mont Aigual (peak culminating at 1565 m corresponding to the southernmost wake). To the east, a sharp shear line separates the Mistral wind from mountain wakes trailing from the western Alps. The high wind zone is more than 300 km long and about 150 km wide with wind speed over 20 m s^{-1} over Saint Chamas. Figures 2b and c zoom on the region documented by the airborne Doppler lidar WIND and compare the simulated (panel b) and measured (panel c) wind fields. The overall simulated structure is in good agreement with the observations. Looking in detail, MM5 underestimates the wind speed, and the shear line is too far to the east which implies that, in the inner domain, MM5 does not show the flow reversal to the east of the shear line.

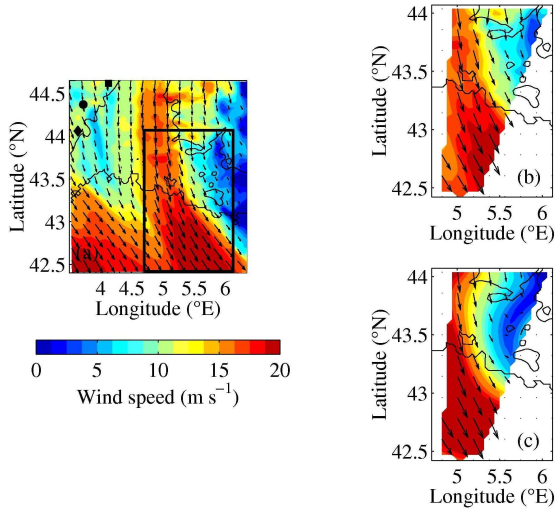

Fig. 2: Horizontal field of horizontal wind at 500 m AGL from MM5 simulations (a). The rectangle indicates the region where the airborne Doppler lidar flew. Panel b is the same as panel a but zoomed in the region indicated by the rectangle. The MM5 simulations are interpolated on the grid used to analyze the WIND measurements. Panel c is the same as panel b but for the observed wind field.

In vertical planes, Fig. 3 displays the wind field measured along legs A-B and C-D (see Fig. 1) by the airborne Doppler lidar WIND (Fig. 3a and c) and the corresponding simulated field (Fig. 3b and d). Arrows indicate the horizontal wind direction as a function of height and the superimposed color map the wind strength. Observations clearly show the north-westerly synoptic wind blowing at about 10 m s^{-1}. In a 1000 m depth layer, the Mistral flow, confined within the PBL depth and experiencing the Rhône valley constriction, blows parallel to the valley axis with an intensity of about 25 m s^{-1} inland (down to 43.7°N). As the Mistral reaches the Rhône valley exist, it decelerates as the Rhône valley enlarges (13 m s^{-1} between 43.2°N and 43.7°N). Along this leg, the MM5 model simulates a weaker deceleration between 43.7 and 43.3°N (see also Fig. 2b). This deceleration is assumed to be associated to a hydraulic jump. Over the Mediterranean (up to 43.2°N), the Mistral accelerates. The horizontal wind field shown in Fig. 2a provides evidence of horizontal convergence over the sea (as the Tramontane and the Mistral flows merge) which results in an acceleration of the Mistral flow over the sea. Other processes such as the change of dynamical roughness associated with the land-sea transition could be responsible for accelerating the Mistral flow over the sea. Along leg B-C, Fig. 3 (panels c and d) evidences the core of the Mistral and the location of the zone of maximum shear that separates the mistral flow from the sheltered zone (43.1°N). It also illustrates the large horizontal inhomogeneity at very small scales. In fact, Aix en Provence is located at about 30 km to the north of Marseille and 30 km to the east of Saint Chamas. Figure 3 shows that the Mistral is maximum over Saint Chamas and that the Mistral flow weakens over Marseille since Marseille is located near the Mistral eastern boundary. Over these two cities, there is a good agreement between the simulations and the observations. At Aix en

Provence (30 km north of Marseille and north-east of Saint Chamas), the Mistral does not blow anymore since Aix en Provence is located near the shearline in the sheltered area in the lee of the western Alps. The MM5 model is here unable to capture this small-scale variability since Fig. 3d shows that the simulated Mistral wind still blows over Aix en Provence that MM5 locates to the west of the Mistral eastern shear line.

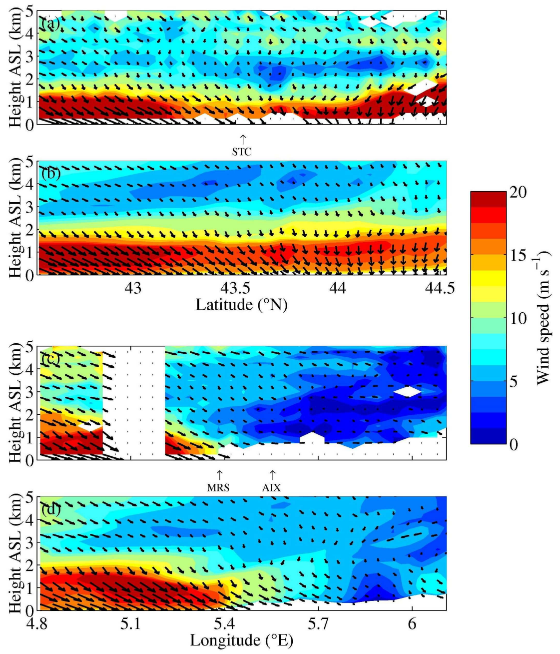

Fig. 3: Wind field along leg A-D and C-D shown in Fig. 1. Panels a and c correspond to the measurements by the airborne Doppler lidar WIND and panels b and d to the simulations. The arrows indicate the locations of the cities of Saint Chamas (STC), Aix en Provence (AIX) and Marseille (MRS).

4.2 *Flow regime analysis*

Investigating the flow regime at the scale of the Rhône valley delta, Fig. 4 shows the simulated 500-m AGL wind speed over the Rhône valley delta with light/dark shades indicating slow/fast flow. In the present case, the flow impinging on the Alpine range and the Massif Central transition to supercritical all along the ridge line, including the Rhône valley and continue to accelerate in the lee regions until a hydraulic jump occurs. Hydraulic jumps correspond to a steepening gravity wave coincident with turbulent kinetic energy maximum.

The hydraulic jumps in the lee of the Massif Central and the Alpine ridge lead to the formation of strong wakes behind and close these peaks. The location of hydraulic jump occurences are displayed in dashed lines in Fig. 4 while the Mistral shear line locations are indicated in solid line. Figure 4 shows that in the lee of the Massif Central, the downslope wind accelerates from 7 to 10 m s^{-1} and, associated with the hydraulic jumps, the low-level wind speed then decreases from 10 to 5 m s^{-1}. The Mistral wind is separated from the Tramontane by the Massif Central wake. Figure 4 shows that in the lee of the Alps, the hydraulic jump, is associated to a low-level wind speed decrease of -10 m s^{-1}, from 15 to less than 5 m s^{-1}. In the western Alps wake, Fig. 4 display two consecutive hydraulic jumps due to the several peaks (Devoluy massif and the Montagne de Lure) that perturbs the downslope flow. The Mistral jet takes a cyclonic curvature at the exit of the Rhône valley due to the Genoa cyclone which makes its structure asymmetrical between the Massif Central and the Alps.

The origin of the western Alps wake is rather complicated and possible mechanisms include dissipation due to hydraulic jumps and PBL turbulence (Jiang et al. 2003). In this study, the observations and simulations suggest a combined wall separation/gravity wave breaking mechanisms to explain the western Alps wake. The flow regime for left-right symmetric shallow water flow past circular topography was discussed by Schär and Smith (1993) (hereafter SS93). The flow regime depends on the upstream Froude number *Fr* and the dimensionless mountain height *M*, which is the mountain height (*h*) to the upstream PBL depth (*H*) ratio. The upstream Froude number *Fr* and the dimensionless mountain height *M* are defined by:

$$\begin{cases} Fr = U/\sqrt{g'H} \\ M = h/H \end{cases}$$

where *g'* is the reduced gravity acceleration. In our case, $H \approx 2300$ m, h = 2500~m, $g' \approx 1.3 \times 10^{-1}$ m s^{-2} and $U \approx 10$ m s^{-1}. These values lead to $Fr = 0.58$ and $M = 1.1$. In the SS93 regime diagram, this corresponds to a wake regime associated with the formation of a hydraulic jump (their regime IIb, see their Fig. 3) and to a wake regime characterized by the inability of the flow to go over the hilltop and, correspondingly, the presence of a stagnation point on the windward slope and the occurence of flow separation (their regime III). The two regimes include reverse flow in the wake. Figures 2 clearly shows the separation of the Mistral flow from the eastern flank of the Rhône valley at about 44°N and the reverse flow in the wake. In SS93, the separation point is associated to a "flank-shock" which is an oblique hydraulic jump meaning that the downstream Froude number is supercritical. In fact, in the Rhône valley, Fig. 4 shows that the hydraulic jump is comparatively smoother than those found downstream of mountain peaks and does not correspond to a brutal return to subcritical regime. This jump is however still associated to flow deceleration (from 20 to 10 m s^{-1} at 500 m AGL and from 12 to 8 m s^{-1} at the surface). Figure 4 also shows in dashed line the hydraulic jump occurring perpendicularly to the eastern valley sidewall at the precise location of the Mistral flow separation (44°N). However, the present situation is similar to the transient regime of SS93 simulations. For a steady-state separation point, the flow on both side of the shear line after the flank-shock should be subcritical, which is not the case for the Mistral flow which is obviously supercritical downstream the flank-shock. Various reasons can be invoked for this: (i) SS93 investigated the case of an isolated hill; (ii) the Mistral flow is transient. However, in our case, and despite the diurnal evolution of the Mistral, the time for the low-level flow to adjust to the local pressure field is substantially shorter than the time scale of large-scale flow variability, so that steady-state flow assumption should be met; (iii) the surface roughness change due the absence of mountain peaks and to the presence of the Mediterranean (and convergence with the Tramontane) downstream the flank-shock, may accelerate the Mistral flow and transition to supercritical regime. The detailed nature of the Mistral flow downstream the in-valley jump (flank-shock) is still to be investigated.

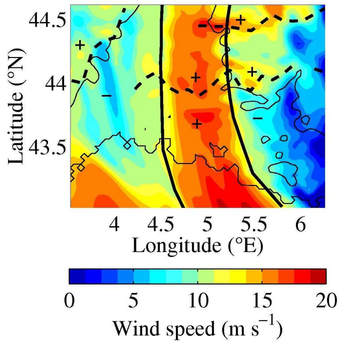

Fig. 4: Simulated 500-m AGL wind speed over the Rhône valley delta. The dashed lines indicate the locations of hydraulic jumps, the solid line shows the eastern and western shear line of the Mistral flow. The signs '+' and '-' correspond to supercritical flow (i.e. local Froude number greater than 1) and subcritical flow (i.e. local Froude number lower than 1), respectively.

5. ACKNOWLEDGMENTS

The authors would like to thank B. Campistron, U. Corsmeier, F. Lohou and R. Vautard for fruitful discussion; M.C Lanceau for help in collecting the referenced papers; B. Cros and P. Durand for the coordination of the experiment; M.P. Lefebvre for her a crucial role in the delicate organization of the flights; E. Nagel for assistance in operation of the WIND system, the pilots of the DLR flight facility, the Falcon technician and the support of the CAATER facilator A. Giez. The flights of the DLR Falcon were funded partly by the CAATER program of the European Commission.

6. REFERENCES

Cros, B., Durand, P., Cachier, H., Drobinski, P., Frejafon, E., Kottmeier, C., Perros, P. E., Peuch, V.-H., Ponche, J.-L., Robin, D., Saïd, F., Toupance, G. and Wortham, H., 2004: The ESCOMPTE program. An overview. *Atmos. Res.*, **69**, 241-279

Grell, G. A., Dudhia, J. and Stauffer, D. R., 1995: A description of the fifth-generation Penn State/NCAR mesoscale model (MM5). NCAR Technical Note, NCAR/TN-398+STR, 122 pp.

Jiang, Q., Smith, R. B. and Doyle, J. D., 2003: The nature of the Mistral: Observations and modeling of two MAP events. *Quart. J. Roy. Meteor. Soc.*, **129**, 857-876

Scialom, G. and Lemaître, Y., 1990: A new analysis for the retrieval of the three-dimensional wind field from multiple Doppler radars. *J. Atmos. Oceanic Technol.*, **7**, 640-665

Schär, C. and Smith, R. B., 1993: Shallow-water flow past isolated topography. Part I: Vorticity production and wake formation. *J. Atmos. Sci.*, **50**, 1373-1400

Werner, C., Flamant, P. H., Reitebuch, O., Köpp, F., Streicher, J., Rahm, S., Nagel, E., Klier, M., Hermann H., Loth, C., Delville, P., Drobinski, P., Romand, B., Boitel, C., Oh, D., Lopez, M., Meissonnier, M., Bruneau, D. and Dabas, A., 2001: Wind infrared Doppler lidar instrument. *Opt. Eng.*, **40**, 115-125